Journal of Solid State Chemistry 184 (2011) 1784–1790

Contents lists available at ScienceDirect

Journal of Solid State Chemistry

journal homepage: www.elsevier.com/locate/jssc

First-principle investigation of Jahn–Teller distortion and topological analysis of chemical bonds in $LiNiO_2$

Zhenlian Chen [a], Huamin Zou [a,b,*], Xiaopeng Zhu [c], Jie Zou [d], Jiefeng Cao [e]

[a] Key Laboratory of Artificial Micro- and Nano-structures of Ministry of Education and School of Physics and Technology, Wuhan University, Wuhan 430072, China
[b] Centre for Electron Microscopy, Wuhan University, Wuhan 430072, China
[c] Information Center of Wuhan Water Group Co. Ltd., Wuhan 430034, China
[d] Physics Department, Eastern Illinois University, Charleston, IL 61920, USA
[e] Shanghai Synchrotron Radiation Facility, Shanghai Institute of Applied Physics, Chinese Academy of Sciences, Shanghai 201800, China

ARTICLE INFO

Article history:
Received 1 November 2010
Received in revised form
14 April 2011
Accepted 18 May 2011
Available online 26 May 2011

Keywords:
$LiNiO_2$
Jahn–Teller distortion
Chemical bonding
AIM
ELF
GGA+U

ABSTRACT

First-principle GGA+U calculations were performed on the undistorted rhombohedral $R\bar{3}m$ model, the collinear Jahn–Teller distorted monoclinic $C2/m$ model, and six non-collinear Jahn–Teller distortion ordering models of $LiNiO_2$. The zigzag and $C2/m$ models are found to be the most stable and the next most stable structural models, respectively. An energy gap appears for the $C2/m$ and zigzag structures, whereas no energy gap appears for the $R\bar{3}m$ structure. Topological analyses were performed on the $R\bar{3}m$, $C2/m$ and zigzag models using the atoms-in-molecules theory and the electron localization function. The results show that the Ni–O interaction is the transit closed-shell interaction, in which the net electron transfer occurs from the Ni ion to the ligand O ions. The Ni–O bond possesses the σ dative bond character and is polarized toward the O ions. In the distorted structures, the bonding electrons around the oxygen atom are strongly polarized toward the long Ni–O bond.

1. Introduction

Due to the difficulty in precisely measuring stoichiometry, the crystal structure of $LiNiO_2$, a promising cathode material, is still a controversial topic. For simplicity, investigations are usually carried out based on the undistorted rhombohedral $R\bar{3}m$ structure. However, crystal structure measurements [1,2] have revealed the Jahn–Teller distortion of the Ni–O octahedron. It has been further suggested that only short-range, local Jahn–Teller distortion exists [1,3]. In previous years, a trimer model was considered to be the best choice based on the pair density function analyses (PDF) of neutron diffraction results [4]. A subsequent investigation of structure factors [5] also suggested that the trimer model was better than the $R\bar{3}m$ structure. However, to the best of our knowledge, no first-principle calculations of the non-collinear Jahn–Teller distortion ordering structures of $LiNiO_2$ have been reported.

The Ni–O bond in $LiNiO_2$ plays an important role not only in the Li^+ intercalation/de-intercalation process [6,7] but also in the magnetic exchange mechanism [8–11]. An insightful depiction of chemical bonding can be obtained by the quantum chemical topology analysis of the electron density with the atoms-in-molecules (AIM) [12] and the electron localization function (ELF) methods [13]. The pictures of a molecular as drawn by the AIM and ELF analyses are complementary. The AIM analysis is based on the topology of the electron density $\rho(\mathbf{r})$, while the ELF analysis is based on the topology of the electron localization function $\eta(\mathbf{r})$, which uses the conditional probability for the same spin pairs and is closely related to the local excess of kinetic energy due to the Pauli repulsion [13,14]. With AIM the three-dimensional space of a molecular is partitioned into disjoint atomic basins, while with ELF the space is partitioned into 'localization basins' such as core basins, lone pair basins and bonding regions [14–20]. The AIM analysis provides the atomic basin population (an indicator of the net charge transfer) [17,19,20], the Laplacian value of the electron density, and the local energy density at the bond critical point (BCP) [12,17,19–27]. In the ELF analysis, the populations of the various basins give rise to a statistical analysis of the bonds, such as, bonding or non-bonding, bond order and bond polarity [14–20], etc.

In the present paper, first-principle GGA+U calculations are performed on the undistorted $R\bar{3}m$ structure, the collinear Jahn–Teller distorted monoclinic $C2/m$ structure, and the six non-collinear Jahn–Teller distortion models. The density of states (DOS) and the difference charge density (DCD) of the $R\bar{3}m$, $C2/m$ and zigzag structures are compared at first. Then, the comprehensive AIM and

* Corresponding author at: Key Laboratory of Artificial Micro- and Nano-structures of Ministry of Education and School of Physics and Technology, Wuhan University, Wuhan 430072, China. Fax: +86 27 68752569.
E-mail address: hmzou@whu.edu.cn (H. Zou).

0022-4596/$ - see front matter © 2011 Elsevier Inc. All rights reserved.
doi:10.1016/j.jssc.2011.05.024

ELF topological analyses are carried out in order to obtain deeper understanding of the bonding characteristics of the material.

2. Details of the calculations

The VASP package [28–32] with PAW-GGA pseudopotential [33,34] and the traditional approach of Liechtenstein et al. [35] were applied in the present calculations. The Coulomb and exchange parameters, U and J, were set to 5.0 and 0.5 eV, respectively, according to the GGA+U calculations of $NaNiO_2$ [9].

In the topological analyses of the charge density, a modified centered difference formula with 4th-order error was used to obtain the first and second derivatives of the charge density grid. This formula was derived based on the Taylor expansion of the charge density on the non-orthogonal grid built by VASP. The grid interval for both the grids of charge density and ELF is about 0.02 Å along each lattice basis vector. The basin partitioning algorithm proposed for Topmod package [36] was applied.

In addition, the following three types of magnetic ordering were considered in the calculations: (1) ferromagnetic ordering (FM); (2) A-type anti-ferromagnetic ordering (A-AFM), i.e., intra-plane FM and inter-plane AFM; (3) C-type AFM (C-AFM), i.e., intra-plane AFM and inter-plane FM. Our calculations show that FM ordering is favorable in the $R\bar{3}m$ structure (about 10 meV/atom lower than the energy of A-AFM and C-AFM ordering). However, for the distorted structures, the energy difference between the three types of magnetic ordering is indiscernible (less than 1 meV/atom). Therefore, the present paper shows only the results of FM in $LiNiO_2$.

3. Jahn–Teller distortion ordering and total energy calculations

Full relaxation here means that the lattice parameters and the ion coordinates are relaxed within the limits of the corresponding space group symmetry. Full relaxation was first performed for the undistorted rhombohedral $R\bar{3}m$ structure shown in Fig. 1(a) and the collinear distorted $C2/m$ structure shown in Fig. 1(b). The total energy of the $C2/m$ structure is about 25 meV/atom lower than that of the $R\bar{3}m$ structure. This value is much larger than the result of the previous GGA calculation (11 meV per formula unit, i.e., about 3 meV/atom) [37].

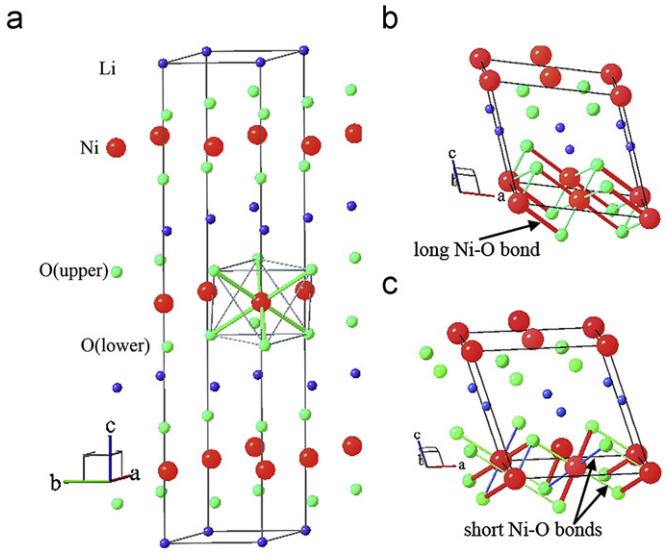

Fig. 1. Structures of $LiNiO_2$: (a) $R\bar{3}m$. (b) $C2/m$. (c) Zigzag. The red balls denote Ni ions, while the green and small blue ones are oxygen ions and Li ions, respectively. In (b), the red lines denote long Ni–O bonds while the green lines are short Ni–O bonds. In (c), the red lines denote long Ni–O bonds while the green and blue lines are the shortest Ni–O bonds and the next shortest bonds, respectively. (For interpretation of the references to color in this figure legend, the reader is referred to the web version of this article.)

Six non-collinear Jahn–Teller distortion models, i.e., the zigzag, dimer, windmill, honeycomb, trimer and altering trimer models are built by shifting the oxygen ions parallel or perpendicular to the flat oxygen planes based on the full relaxed $R\bar{3}m$ structure. All models, except the dimer model, were investigated with the pair density function (PDF) analysis based on the neutron diffractions by Chung et al. [4]. The sketches of these models are redrawn with the software Balls & Sticks (BS) [38] as shown in Fig. 2, in which only the shifted oxygen ions are linked with the Ni ions. The oxygen ion, which is shared by three marked Ni–O bonds in the honeycomb model, the trimer model and the altering trimer model, shifts perpendicularly to the flat oxygen plane, i.e. along the **c** axis of the $R\bar{3}m$ hexagonal lattice. In the dimer model, the oxygen ion lying on the upper plane and shared by two marked Ni–O bonds shifts along $\mathbf{T}_1$ ($\mathbf{a}+2\mathbf{b}$) direction, while the one lying on the lower plane and shared by two marked Ni–O bonds shifts along $\mathbf{T}_4$ ($-\mathbf{a}-2\mathbf{b}$) direction. Here, the vectors **a, b** and **c** are the basis vectors of the hexagonal lattice unit cell of the $R\bar{3}m$ model. The vectors $\mathbf{T}_1$, $\mathbf{T}_2$….$\mathbf{T}_6$ are defined in Fig. 2. Other oxygen ions linked to the Ni ions marked by black-gray lobes in Fig. 2 are shifted along the projection direction of the Ni–O bond from Ni ion to O ion on the oxygen plane, e.g., the upper oxygen ions in the $C2/m$ model (see Fig. 2(c)) shift along $\mathbf{T}_4$ ($-\mathbf{a}-2\mathbf{b}$) direction. In the zigzag model, all the oxygen ions are shifted parallel to the flat oxygen plane, while in the dimer and windmill models, the fractions of the shifted oxygen ions are half and three fourth, respectively. In the honeycomb model, no shift parallel to the plane happens, and one fourth of the oxygen ions in each oxygen plane are jostled out of the flat plane. In the trimer model, one third of the oxygen ions in the upper oxygen plane are lifted and all the oxygen ions in the lower oxygen plane are shifted parallel to the plane. For the altering trimer model, in each oxygen plane, one sixth of the oxygen ions are jostled out of the flat plane and half of the oxygen ions are shifted parallel to the plane.

To calculate the total energy as a function of the bond length, the length of the marked Ni–O bonds is adjusted by shifting the oxygen ions with an interval of ($0.01\mathbf{T}_i$, $0.005\mathbf{T}_c$) within a range of ($-0.1\mathbf{T}_i \sim +0.1\mathbf{T}_i$, $-0.05\mathbf{T}_c \sim +0.05\mathbf{T}_c$). Here, $\mathbf{T}_i$ ($i=1,2,\ldots,6$) are parallel to the flat oxygen plane and defined as $\mathbf{T}_1=\mathbf{a}+2\mathbf{b}$; $\mathbf{T}_2=2\mathbf{a}+\mathbf{b}$; $\mathbf{T}_3=-\mathbf{a}+\mathbf{b}$; $\mathbf{T}_4=-\mathbf{a}-2\mathbf{b}$; $\mathbf{T}_5=-2\mathbf{a}-\mathbf{b}$; $\mathbf{T}_6=\mathbf{a}-\mathbf{b}$. The vector $\mathbf{T}_c$ denotes the direction vector of the shift along **c** axis ($\mathbf{T}_c=\mathbf{c}$ for the upper oxygen ions and $\mathbf{T}_c=-\mathbf{c}$ for the lower oxygen ions), based on the $R\bar{3}m$ hexagonal lattice. The calculated Ni–O bond length and the corresponding total energy in the most stable state are obtained and listed in the upper part of Table 1. The common character among the trimer, altering trimer and honeycomb models is that there exist trimers composed of three equivalent Ni–O bonds. The total energies of these three models are all higher than that of the $R\bar{3}m$ structure. The total energy of the zigzag model is 22 meV/atom lower than that of the $R\bar{3}m$ structure, which indicates that the zigzag model is unambiguously superior to the $R\bar{3}m$ structure. As listed in Table 1, the calculated total energies indicate that the other two models, i.e., the dimer model and the windmill model, are better than the $R\bar{3}m$ structure, but worse than the zigzag model. In the most stable state of both the zigzag and dimer models, the marked Ni–O bonds are elongated. However, in the most stable state of the windmill model, the Ni–O bonds marked in Fig. 2(f) are shortened, and the length of the Ni–O bonds of the undistorted NiO_6 octahedron in this model (the center Ni site not being marked by black-gray lobes) is 2.02 Å. In contrast, in the next most stable

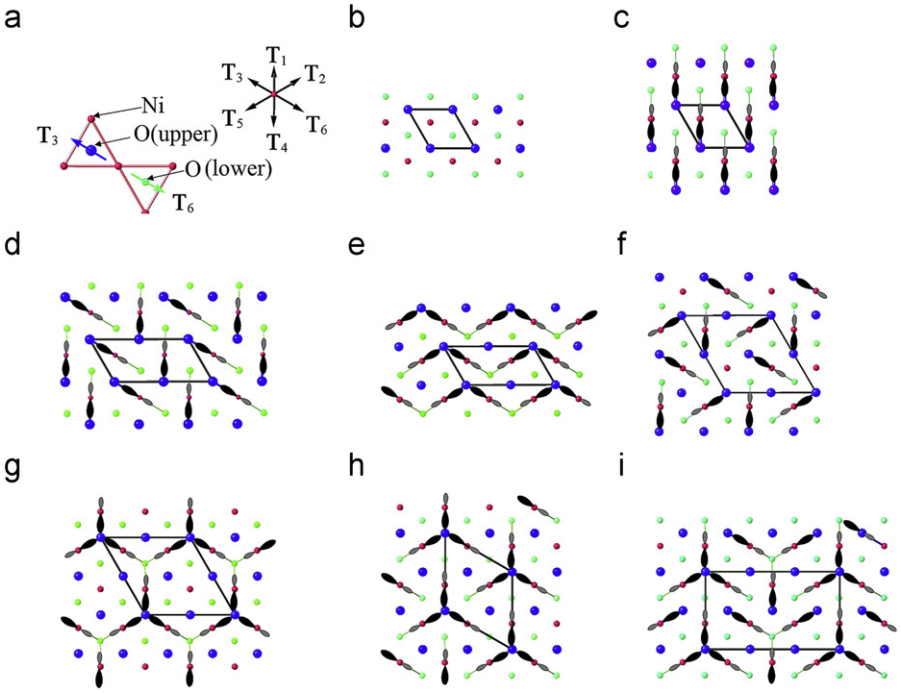

Fig. 2. Models viewed along the **c** axis. The red balls denote Ni ions, the blue and green balls are oxygen ions in the upper plane and in the lower plane, respectively. Only the shifted oxygen ions are linked with the Ni ions in the sketches. The unit cell of each model is outlined with black lines. (a) Definitions of the six shift directions in the flat oxygen plane: $\mathbf{T}_1=\mathbf{a}+2\mathbf{b}$; $\mathbf{T}_2=2\mathbf{a}+\mathbf{b}$; $\mathbf{T}_3=-\mathbf{a}+\mathbf{b}$; $\mathbf{T}_4=-\mathbf{a}-2\mathbf{b}$; $\mathbf{T}_5=-2\mathbf{a}-\mathbf{b}$; $\mathbf{T}_6=\mathbf{a}-\mathbf{b}$. Vectors **a, b** and **c** are the basis vectors of the $R\bar{3}m$ hexagonal lattice. (b) $R\bar{3}m$. (c) $C2/m$. (d) Zigzag. (e) Dimer. (f) Windmill. (g) Honeycomb. (h) Trimer. (i) Altering trimer.

Table 1
The Ni–O bond lengths and the total energies (the unit is meV/atom) of the non-collinear Jahn–Teller distortion models within rhombohedral lattice basis. The shift of the oxygen ion along the appointed direction (shown in Fig. 2(a)) in the oxygen plane is ($x\mathbf{T}_i$, $0.5x\mathbf{T}_c$). The data for the full relaxed $R\bar{3}m$, $C2/m$ and zigzag structures are also given.

Model	Ni–O(Å)	x	E
Zigzag	1.92,2.11	0.03	−22
Dimer	1.89,1.98,2.02	0.02	−6
Windmill	1.89,1.98,2.02	−0.02	−11
Windmill[1]	1.94,1.98,2.06	0.02	−6
honeycomb	1.98,2.06	0.02	9
trimer	1.94,1.98,2.06	0.02	5
alter-trimer	1.94,1.98,2.06	0.02	6
$R\bar{3}m^{fr}$ (hexagonal)	1.98 a=2.88 Å, c=14.32 Å;	Li:3a; Ni:3b; O: 6c(0,0,0.241)	0
$C2/m^{fr}$ ($C12/m1$)	1.90,2.15 a=5.16 Å, b=2.79 Å, c=5.13 Å; β=111.95°	Li:2d; Ni:2a; O:4i(0.277,0,0.776)	−25
Zigzag^{fr} ($P12_1/a1$)	1.90,1.91,2.12 a=4.92 Å, b=2.93 Å, c=4.99 Å; β= 107.87°	Li:2b; Ni:2a; O: 4e(0.249,0.449,0.222)	−29

The energy of the $R\bar{3}m$ structure is chosen as zero. The superscript ^{fr} represents full relaxation. In the windmill model the Ni–O bonds marked with black-gray lobes in Fig. 1(c) are shortened. Windmill[1] represents the state in which the marked Ni–O bonds are elongated. The data of the honeycomb, trimer and altering trimer models listed in this table are for reference only.

state labeled as windmill[1], the marked Ni–O bonds are elongated, and the length of the Ni–O bonds of the undistorted NiO_6 octahedron in this model is 1.94 Å.

The energy gain of the Ni ion due to the Jahn–Teller distortion is important and easily understood since the e_g orbitals are not fully occupied. However, in the windmill models and the honeycomb model, part of the Ni ions, which sit in the undistorted NiO_6 octahedrons and are not marked by black-gray lobes, may not obtain this part of energy gain. In addition to the energy gain of Ni ions, the energy gain of the oxygen ion from removing the degeneracy of the O-2p orbitals is also important. First, it will be shown in the following chapter that the oxygen atomic basin population is about 7e, i.e., the O-2p orbitals are also not fully occupied. In the $R\bar{3}m$ structure, the three O-2p orbitals are degenerated and equally occupied. However, in the $C2/m$ and zigzag models, the electrons are more highly localized in the long Ni–O bond than in the short Ni–O bonds, which induces the energy gain from the split of the O-2p orbitals. Second, in the $C2/m$ and zigzag models shown in Fig. 2(c)–(d), the O-2p orbitals are split for every oxygen ion. Whereas, in the other five Jahn-Teller distortion ordering models shown in Fig. 2(e)–(i), part of the oxygen ions are un-shifted and then the three Ni–O bonds are equivalent. Meanwhile, in the honeycomb, trimer and altering trimer models, another part of the oxygen ions, i.e., the ones

jostled out the oxygen plane, are also shared by three equivalent Ni–O bonds. These oxygen ions may not obtain the energy gain since the three 2*p* orbitals are almost degenerated and equally occupied. In a word, both the energy gain contributions from Ni-e_g orbital split and from O-2*p* orbital split might be the main reasons that the *C*2/*m* and zigzag models are superior to the other models.

The zigzag model shown in Figs. 1(c) and 2(d) belong to the space group $P2_1/c$ (No.14). After full relaxation, which does not break the Jahn–Teller distortion ordering, the total energy of the zigzag structure is about 4 meV/atom lower than that of the *C*2/*m* structure. An energy gap near the Fermi level appears in the DOS curves for both the *C*2/*m* and zigzag structures, while no gap appears in the DOS curve for the $R\bar{3}m$ structure, as shown in Fig. 3. Our result for the $R\bar{3}m$ structure is consistent with the previous LDA+U calculation which showed that $LiNiO_2$ is a metal [39] with the $R\bar{3}m$ structure. However, the self-interaction corrected local spin-density method (SIC-LSD) showed an energy gap of about 1.4 eV [40] in the $R\bar{3}m$ structure. The photoemission experiment suggested a gap of 0.4 eV in $LiNiO_2$ as mentioned by Anisimov et al. [39]. Our results show that the width of the energy gap is about 0.25 eV for the *C*2/*m* structure and about 0.35 eV for the zigzag structure, respectively, which are much closer to the experimental result than the result of the SIC-LSD calculation [40].

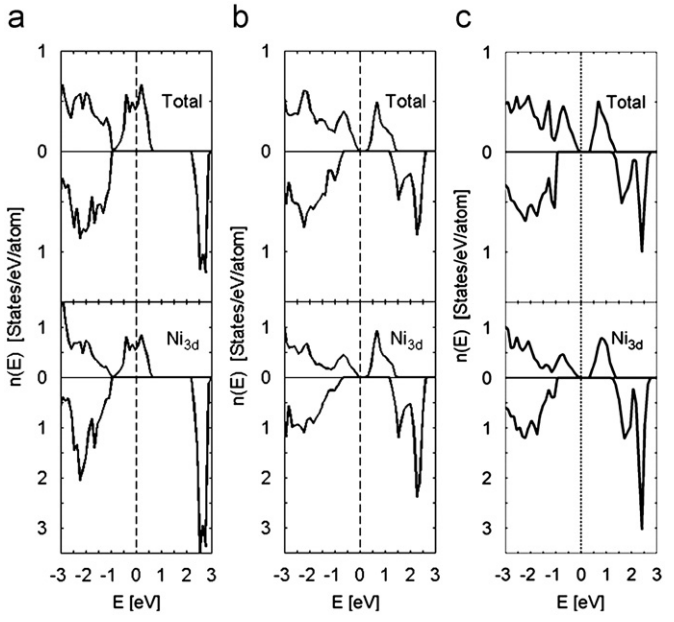

Fig. 3. The spin-decomposed density of states for different structural models of $LiNiO_2$. The dashed line indicates the position of the Fermi level. (a) With the $R\bar{3}m$ model. (b) With the *C*2/*m* model. (c) With the zigzag model.

4. Valence charge density and electron localization function in the $R\bar{3}m$, *C*2/*m* and zigzag structures

4.1. Difference charge density isosurfaces

Difference charge density (DCD) is defined here as the remainder after a superposition of atomic charge densities is subtracted from the total charge density calculated self-consistently. The isosurfaces of four values, −0.4, 0.1, 0.2 and 0.3 e/Å^3 (blue, green, magenta, and red, respectively) are shown in Fig. 4. The blue balloon-shaped domains, which come from the Ni ion and point to the ligand O ions, denote the decrease in the population of the $3d_{x^2-y^2}$ orbital and the $3d_{z^2}$ orbital. The green bean-shaped domains around the Ni ion express the increase in the population of the $3d_{xy}$, $3d_{yz}$, $3d_{xz}$ orbitals. These indicate that the degenerate 3*d* orbitals are split into the e_g and t_{2g} orbitals due to the octahedral crystal field. In the distorted structures, as indicated by the volume of the blue balloon-shaped domains, the decrease in the population of the $3d_{x^2-y^2}$ orbital is slightly larger than that of the $3d_{z^2}$ orbital as expected, when the z axis is parallel to the long Ni–O bond. Around each oxygen ion, there is one magenta ball-shaped domain in the $R\bar{3}m$ structure and one magenta peanut-shaped domain in each distorted structure. The red core-shaped domain in the magenta peanut-shaped domain suggests very high localization of electrons (in the $R\bar{3}m$ structure, the red core-shaped domain is obscured by the magenta ball-shaped domain in Fig. 4(a)).

4.2. Topological analysis of the valence charge density at BCPs

Table 2 lists the topological characteristics of the Ni–O bonds at BCPs, including $\rho(\mathbf{r})_{bcp}$ and $\nabla^2\rho(\mathbf{r})_{bcp}$, the distance from the BCP to the related Ni ion (d1) and that to the related O ion (d2), and the local energy density, $H(\mathbf{r})$. It can be seen that the BCPs are closer to the Ni ions than to the O ions. The ellipticity values ε are very close to zero (<0.08), which means that the σ-bond components are dominant. The small $\rho(\mathbf{r})_{bcp}$ and the positive Laplacian values indicate the depletion of charge densities at the BCPs. These are in good agreement with the AIM analysis result derived from the QCBED experiment [27]. In the present work, the local energy density, $H(\mathbf{r})$, which is used to characterize the interatomic interactions in combination with the Laplacian value [26],

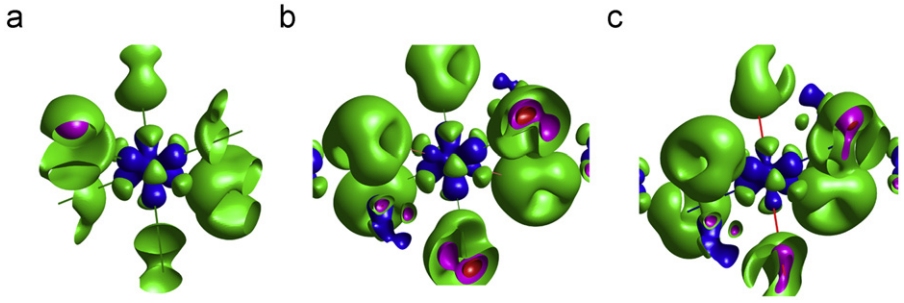

Fig. 4. Difference charge density isosurfaces of an oxygen octahedron with a Ni ion at the center for the $R\bar{3}m$, *C*2/*m* and zigzag structures, respectively. The isosurfaces of DCD=0.3, 0.2, 0.1, and −0.4 e/Å^3 are shown in red, magenta, green and blue, respectively. (a) The $R\bar{3}m$ structure. (b) The *C*2/*m* structure. The long Ni–O bonds are marked with red lines and the short bonds are marked with green lines. (c) The zigzag structure. The long Ni–O bonds are marked with red lines, the shorter Ni–O bonds are marked with green lines, and the shortest Ni–O bonds are marked with blue lines. (For interpretation of the references to color in this figure legend, the reader is referred to the web version of this article.)

Table 2
Topological characteristics at BCPs of the Ni–O bonds in the $R\bar{3}m$ structure, $C2/m$ structure and zigzag structure.

Object	Bond	($d1$,$d2$) (Å)	$\rho(\mathbf{r})$ (eÅ^{-3})	$\nabla^2\rho(\mathbf{r})$ (eÅ^{-5})	$H(\mathbf{r})$ (kJ mol^{-1} per atomic unit volume)	BD (Hartree/e)	ε
$R\bar{3}m$	Ni–O	0.905,1.074	0.521	10.406	−10.977	−0.054	0.012
$C2/m$	Ni–O1	0.869,1.029	0.627	14.086	−15.985	−0.066	0.043
	Ni–O2	1.011,1.136	0.372	3.345	−29.806	−0.206	0.051
Zigzag	Ni–O1	0.866,1.037	0.622	14.809	−7.250	−0.030	0.081
	Ni–O2	0.870,1.036	0.616	13.975	−12.792	−0.053	0.013
	Ni–O3	0.929,1.195	0.388	3.809	−30.021	−0.199	0.030

Table 3
Basin populations.

Object	A(Ni)	A(O)	V(O)	C(Ni)	V(Ni)	V(Ni, O)		
						Total	|O	|Ni
$R\bar{3}m$	8.66	7.17	3.58	0.34	6.28	1.54	1.21	0.32
$C2/m$	8.67	7.17	3.41	0.35	7.06	4.32	3.75	0.57
Zigzag	8.65	7.18	3.66	0.35	6.58	4.37	3.60	0.76

The label, V(Ni,O), represents one Ni–O bond basin in the $R\bar{3}m$ structure and the whole domain including all three bond basins around the O ion in each distorted structure. The contribution from the Ni atomic basin to the population V(Ni, O)|Ni of the longest Ni–O bond is nearly zero, thus the populations V(Ni, O)|Ni almost entirely come from the Ni atomic basins of the short Ni–O bonds. The population C(Ni) is the contribution of the 3*d* subshell to the core basin.

is also calculated following Presti and Destro [25]. The ratio, $H(\mathbf{r})_{bcp}/\rho(\mathbf{r})_{bcp}$, which can be used as a bond degree (BD) parameter [26], is also listed in Table 2. For all the Ni–O bonds, the $\nabla^2\rho(\mathbf{r})_{bcp}$ values are positive and the $H(\mathbf{r})_{bcp}$ values are negative, which is an indication of the transit closed-shell interaction between the Ni ions and the O ions. The BD values of the Ni–O bonds in the $R\bar{3}m$ structure and the short Ni–O bonds in the two distorted structures are very small negative numbers, while the absolute values of the BD parameter of the longer Ni–O bonds are about three times those of the shorter Ni–O bonds.

The atomic basin population of the Ni ion, as listed in Table 3, is about 8.7e. The total number of valence electrons of a Ni atom considered in the pseudopotential is 10. Thus about 1.3 electrons are transferred from each Ni ion to six ligand O ions. The Li ion is fully ionized, and its electron is transferred to the six nearest O ions. The total number of electrons of an O atom considered in the pseudopotential is 6, and one O ion is connected to three Ni ions and three Li ions. Thus, about 1.2 electrons are transferred to each O ion, as also shown in Table 3. The fact that the Ni–O transit closed-shell interaction involves the electron transfer from the metal to the ligand oxygen ions indicates the dative character of the Ni–O bond [19].

4.3. Topological analysis of the ELF function

In Fig. 5, the isosurfaces of ELF = 0.65 for the $R\bar{3}m$ structure and those of ELF = 0.70 for the two distorted structures show that the lone pair basin of each O ion is located on the opposite side of the oxygen ion with respect to the Ni–O bonds. The lone pair basin contains nearly two electron pairs, as shown in Table 3 by the values of V(O). In the $R\bar{3}m$ structure there are three equivalent bond attractors, and the distance from each bond attractor is about 0.6 Å to the O ion and about 1.4 Å to the Ni ions. Since the Ni–O BCPs are closer to the Ni ions than to the O ion, the Ni–O bond attractors are located within the oxygen atomic basin, and the Ni–O bonds are polarized toward the O ion. The population of each bond basin is about 1.5 electrons. About 79% of the population of the bond basin V(Ni,O) comes from the contribution of the oxygen atomic basin, which also indicates the highly polarized dative bond character of the Ni–O bond [19].

Similar to the $R\bar{3}m$ structure, in the zigzag structure the bond attractors are also closer to the O ions than to the Ni ions by about half the distances to the Ni ions, whereas the BCPs of the Ni–O bonds are closer to the Ni ions. This means that the Ni–O bond attractors are all located within the oxygen atomic basin and the Ni–O bonds are polarized toward the O ion. The calculated bond basin populations of the next shortest and the shortest Ni–O bonds are 0.60e and 0.45e, respectively. The bond basin population of the long Ni–O bond is 3.32 e. The main difference in the ELF topology of the zigzag structure from that of the $R\bar{3}m$ structure is that the two short Ni–O bonds are very weak and the associated bond attractors correspond to the very shallow maxima of ELF, whereas the long Ni–O bond is very strong, as seen in Figs. 5(c), (d) and 6(c). Some electrons of the two short Ni–O bond basins are delocalized to the high ELF areas of the long Ni–O bond and the oxygen lone pair. Calculated populations show that about 0.1e of the long Ni–O bond basin come from the Ni atoms of the short Ni–O bonds. This is similar to the case of the OSSSO, in which the S1–S3 bond is weak and the associated bond basin is absent [41], or the case of NO_2, in which the comma-shaped nitrogen lone pair basin points to and partially overlaps into the N–O bond basin [42]. The case of the $C2/m$ structure is quite similar to that of the zigzag structure. The short Ni–O bonds in the $C2/m$ structure seem so weak that the short Ni–O bond attractor is invisible, as shown in the contour map of Fig. 6(b). The population of the whole domain including all three Ni–O bonds in each distorted structure is labeled as V(Ni,O) in Table 3. It can be seen that in the $C2/m$ structure about 87% of the electrons in the ELF domain come from the oxygen atomic basin, and that fraction in the zigzag structure is about 82%. Almost all the remaining electrons are from the nickel atomic basins of the short Ni–O bonds, and the contribution from the nickel atomic basin of the long Ni–O bond is nearly zero. This indicates the pure dative bond character of the long Ni–O bond.

The 3*d* subshell has an ambivalent character of sharing both the core and valence basins [19,20]. About 0.35 valence electrons of Ni are distributed in the core basin. The other non-bonding electrons of the Ni ion are distributed in eight valence basins, whose attractors are located about 0.85 Å away from the Ni nucleus in the green bean-shaped domains avoiding the Ni–O bonds (see Fig. 4). The total number of the non-bonding electrons

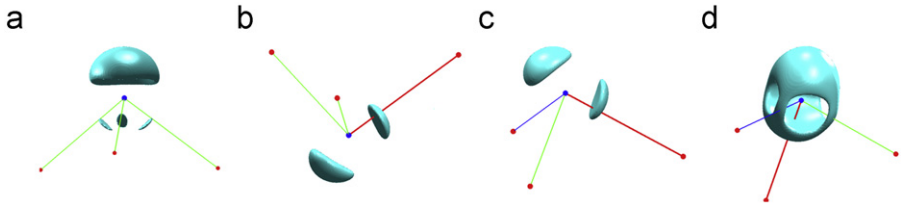

Fig. 5. Isosurfaces of ELF around an oxygen atom and its three nearest neighboring Ni atoms. (a) ELF=0.65 in the $R\bar{3}m$ structure. (b) ELF=0.70 in the $C2/m$ structure. The long Ni–O bond is displayed in red and the short ones are displayed in green. (c) ELF=0.70 in the zigzag structure. (d) ELF=0.62 in the zigzag structure. The Ni–O bonds in the zigzag structure with the length of 2.12, 1.91 and 1.90 Å are displayed in red, blue and green, respectively. (For interpretation of the references to color in this figure legend, the reader is referred to the web version of this article.)

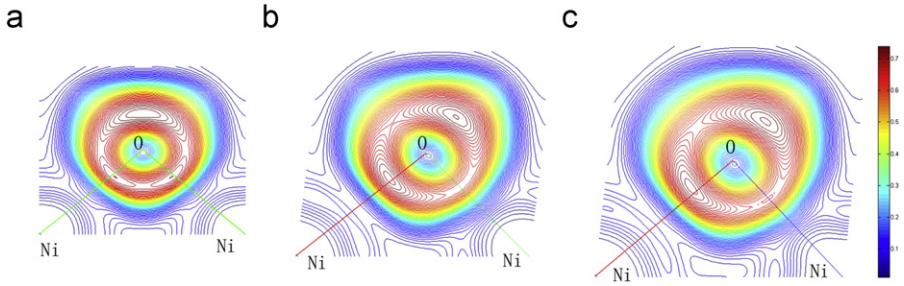

Fig. 6. Contour maps with 0.01 interval of ELF on the Ni–O plane, in which two Ni–O bonds lie on the plane and the third Ni–O bond is out of this plane. (a) In the $R\bar{3}m$ structure. (b) In the $C2/m$ structure. The long Ni–O bond is marked with the red line and the short Ni–O bond is marked with the green line. (c) In the zigzag structure. The long Ni–O bond is marked with the red line and the next shortest bond is marked with the blue line. (For interpretation of the references to color in this figure legend, the reader is referred to the web version of this article.)

of the Ni ion is about 6.6, 7.4 and 6.9 in the $R\bar{3}m$, $C2/m$ and zigzag structures, respectively. The total number of valence electrons of a Ni atom considered in the pseudopotential is 10. The polarity of the Ni–O bonds is toward the O ions. These suggest that the valence of the Ni ion is about +3.4 in the $R\bar{3}m$ structure, +2.6 in the $C2/m$ structure, and about +3.1 in the zigzag structure.

5. Conclusion

According to the calculated total energies, the two Jahn–Teller distorted structures, i.e., the $C2/m$ structure and the zigzag distortion ordering model, are clearly much more stable than other structural models of $LiNiO_2$. The structure with the zigzag model of Jahn–Teller distorted ordering is even more stable than the $C2/m$ structure from the point of view of the total energy. The energy gap appearing near the Fermi level in the DOS curve is 0.25 eV in the $C2/m$ structure and 0.35 eV in the zigzag model, which indicates that the material $LiNiO_2$ with the above two structures is a semiconductor. However, no energy gap is found in the $R\bar{3}m$ structure, which indicates that the compound $LiNiO_2$ with this structure is a metal. The DCD calculations show that due to the crystal field effect, the 3d level is split into the e_g and t_{2g} sublevels, and the e_g sublevel is further split into $3d_{z^2}$ and $3d_{x^2-y^2}$ in the distorted structures. The Li ions are fully ionized. About 1.3 electrons are transferred from each Ni atom to the ligand O atoms. The Ni–O interaction belongs to the transit closed-shell interaction. The Ni–O bonds are σ dative bonds and most of the bonding electrons come from the oxygen atomic basin. In the distorted structures, the bonding electrons around the oxygen atom are strongly polarized toward the long Ni–O bond. At the same time, the short Ni–O bonds are so weak that the long Ni–O bond basin and the oxygen lone pair basin are overlapped into the region of the basins of the short bonds. Due to the coexistence of the charge transfer and polarized covalent bonding between Ni and O, the valence of the Ni ion for the studied structural models of $LiNiO_2$ is close to +3.

Acknowledgments

This work is supported financially by the National Natural Science Foundation of China (No. 50671073). The authors are grateful to Dr. Steven L. Mullen for valuable suggestions during the preparation of the manuscript.

Appendix A. Supporting information

Supplementary data associated with this article can be found in the online version at doi:10.1016/j.jssc.2011.05.024.

References

[1] A. Rougier, C. Delmas, A.V. Chadwick, Solid State Commun. 94 (1995) 123–127.
[2] I. Nakai, K. Takahashi, Y. Shiraishi, T. Nakagome, F. Nishikawa, J. Solid State Chem. 140 (1998) 145–148.
[3] C. Pouillerie, E. Suard, C. Delmas, J. Solid State Chem. 158 (2001) 187–197.
[4] J.H. Chung, T. Proffen, S. Shamoto, A.M. Ghorayeb, L. Croguennec, W. Tian, B.C. Sales, R. Jin, D. Mandrus, T. Egami, Phys. Rev. B 71 (2005) 064410-1-11.
[5] J. Cao, H. Zou, C. Guo, Z. Chen, S. Pu, Solid State Ionics 180 (2009) 1209–1214.
[6] Y. Koyama, Y.-S. Kim, I. Tanaka, H. Adachi, Jpn. J. Appl. Phys. 38 (1999) 2024–2027.
[7] S. Chabaud, C. Bellin, F. Mauri, G. Loupias, S. Rabii, L. Croguennec, C. Pouillerie, C. Delmas, T. Buslaps, J. Phys. Chem. Solids 65 (2004) 241–243.
[8] M.V. Mostovoy, D.I. Khomskii, Phys. Rev. Lett. 89 (2002) 227203-1-4.
[9] H. Meskine, S. Satpathy, Phys. Rev. B 72 (2005) 224423-1-9.
[10] A.J.W. Reitsma, L.F. Feiner, A.M. Oles, New J. Phys. 7 (2005) 121-121.
[11] I.I. Mazin, Phys. Rev. B 75 (2007) 094407-1-5.
[12] R.F.W. Bader, Atoms in Molecules: a Quantum Theory, Oxford University Press, Oxford, 1990.
[13] A.D. Becke, K.E. Edgecombe, J. Chem. Phys. 92 (1990) 5397–5403.
[14] B. Silvi, A. Savin, Nature 371 (1994) 683–686.
[15] A. Savin, B. Silvi, F. Coionna, Can. J. Chem. 74 (1996) 1088–1096.
[16] S. Raub, G. Jansen, Theo. Chem. Acc. 106 (2001) 223–232.
[17] R. Llusar, A. Beltran, J. Andres, F. Fuster, B. Silvi, J. Phys. Chem. A 105 (2001) 9460–9466.
[18] B. Silvi, J. Mol. Struct. 614 (2002) 3–10.
[19] J. Pilme, B. Silvi, M.E. Alikhani, J. Phys. Chem. A 107 (2003) 4506–4514.
[20] E. Matito, M. Sola, Coord. Chem. Rev. 253 (2009) 647–665.

[21] R.F.W. Bader, Chem. Rev. 91 (1991) 893–928.
[22] Y. Aray, J. Rodriguez, D. Vega, J. Phy. Chem. B 104 (2000) 4608–4612.
[23] G. Gervasio, R. Bianchi, D. Marabello, Chem. Phys. Lett. 387 (2004) 481–484.
[24] J. Reinhold, O. Kluge, C. Mealli, Inorg. Chem. 46 (2007) 7142–7147.
[25] L.L. Presti, R. Destro, J. Chem. Phys. 128 (2008) 044710-9.
[26] E. Espinosa, I. Alkorta, J. Elguero, E. Molins, J. Chem. Phys. 117 (2002) 5529–5542.
[27] J. Cao, C. Guo, H. Zou, J. Solid state Chem 182 (2009) 555–559.
[28] Vasp. 〈http://cms.mpi.univie.ac.at/vasp〉.
[29] G. Kresse, J. Furthmüller, Phys. Rev. B 54 (1996) 11169–11186.
[30] G. Kresse, J. Furthmüller, Comp. Mater. Sci. 6 (1996) 15–50.
[31] G. Kresse, J. Hafner, Phys. Rev. B 47 (1993) 558–561.
[32] G. Kresse, J. Hafner, Phys. Rev. B 49 (1994) 14251–14269.
[33] P.E. Blochl, Phys. Rev. B 50 (1994) 17953–17979.
[34] G. Kresse, D. Joubert, Phys. Rev. B 59 (1999) 1758–1775.
[35] A.I. Liechtenstein, V.I. Anisimov, J. Zaanen, Phys. Rev. B 52 (1995) R5467–R5470.
[36] S. Noury, X. Krokidis, F. Fuster, B. Silvi, Comput. Chem. 23 (1999) 597–604.
[37] C.A. Marianetti, D. Morgan, G. Ceder, Phys. Rev. B 63 (2001) 224304-1-15.
[38] P.W. Anderson, Mater. Res. Bull. 8 (1973) 153–160.
[39] V.I. Anisimov, J. Zaanen, O.K. Andersen, Phys. Rev. B 44 (1991) 943–954.
[40] L. Petit, G.M. Stocks, T. Egami, Z. Szotek, W.M. Temmerman, Phys. Rev. Lett. 97 (2006) 146405-1-4.
[41] D.B. Chesnut, L.J. Bartolotti, R.D. Harcourt, J. Phys. Chem. A 113 (2009) 8677–8682.
[42] D.B. Chesnut, A.L. Crumbliss, Chem. Phys. 315 (2005) 53–58.